MPI–PhT 99-13
February 1999
hep–ph/9903470

Probing the parton densities of virtual photons with the reaction $\gamma^*\gamma \to$jets at LEP

B. Pötter
Max-Planck-Institut für Physik,
Föhringer Ring 6, 80805 München, Germany.
E-mail: poetter@mppmu.mpg.de

Abstract

We present a next-to-leading order calculation of jet production in $\gamma^*\gamma$ collisions from e^+e^- scattering in a region where the virtuality Q^2 of the probing virtual photon is small compared to the transverse jet energy. The calculation is based on the phase-space slicing method. The initial state singularity of the virtual photon is factorized into the structure function of the virtual photon, using the $\overline{\rm MS}$ factorization scheme for virtual photons. Numerical results are presented for LEP2 conditions. The perturbative stability of the pure direct virtual photon approach is compared to that of including resolved virtual photons in different regions of Q^2. We make predictions for cross sections which suggest that different parametrizations of virtual photon parton densities should be distinguishable by measurements of jet cross sections at LEP.

1 Introduction

Considerable progress has recently been made in investigating the structure of the virtual photon in jet production from eP-scattering at HERA. On the theoretical side calculations are available in leading order (LO) [1] and next-to-leading order (NLO) [2, 3]. An increasing number of experimental data becomes available [5] and the confrontation of these results with the NLO calculations indicates that the concept of a resolved virtual photon, i.e., the virtual photon as a source of quarks and gluons, is necessary to describe the data in the low Q^2 region, where Q^2 is the virtuality of the photon. The parton distribution function (PDF) of the virtual photon is constructed in analogy to that of the real photon, with the difference that the virtual photon PDF has an extra Q^2-dependence built in, in addition to the usual factorization scale dependence. In the limiting case $Q^2 \to 0$, the virtual photon PDF's reproduce the real photon PDF's. Since so far only limited data exist on the structure of the virtual photon [6], the modeling of the Q^2-behaviour of the virtual photon PDF is still rather ambiguous. Two LO parametrizations of the virtual photon PDF are available that fit the data [6], namely those of Glück, Reya and Stratmann [7], which have very recently been updated by Glück, Reya and Schienbein [8] (GRS), and those of Schuler and Sjöstrand [9] (SaS). The GRS group has also calculated the virtual photon PDF's in NLO, but no parametrization is available up to now, since the differences between the LO and NLO parametrizations are small and the available data is not yet very precise.

It is desirable to find alternative ways of probing the virtual photon PDF's, either to test their universality or to further constrain their Q^2-dependence. One possibility is the reaction $\gamma^*(Q^2) + \gamma(P^2 \simeq 0) \to \text{jets}(E_T) + X$, where the virtuality of the probing photon Q^2 has to be sufficiently small in comparison with the transverse jet energy E_T to allow for a hadronic component in the virtual photon. The real photon with virtuality $P^2 \simeq 0$ involved in the collision has both a direct pointlike and a resolved hadronic part. This reaction can be obtained at e^+e^- colliders by single-tag experiments, and preliminary results have been reported from the OPAL collaboration at LEP [10] for $6 \leq Q^2 \leq 30$ GeV^2. For the large Q^2 region we have recently evaluated the NLO QCD corrections to this process and found them to be small and to improve the scale dependence [11]. Moving towards the region of small virtualities, especially for $Q^2 \ll E_T^2$, one expects logarithms from the initial state $\gamma^* \to q\bar{q}$ splitting of the form $\ln(Q^2/s)$, where $\sqrt{s}$ is the partonic center-of-mass energy, to become large and spoil the convergence of the perturbative expansion. A procedure for subtracting these terms from the direct virtual photon cross sections and absorbing them into the PDF of the resolved photon has been worked out for the case of eP-scattering in [2] in the framework of the phase-space-slicing method in analogy to the subtraction of $1/\epsilon$ poles from photoproduction [12, 13]. In section 2 of this paper we will work out the subtraction procedure for the $\gamma^*\gamma$-scattering case, closely following the approach in [2]. With the subtraction performed, one has to include a resolved virtual photon contribution into the jet cross sections. In the deep-inelastic case as described in [11], the virtual photon couples only directly and the real

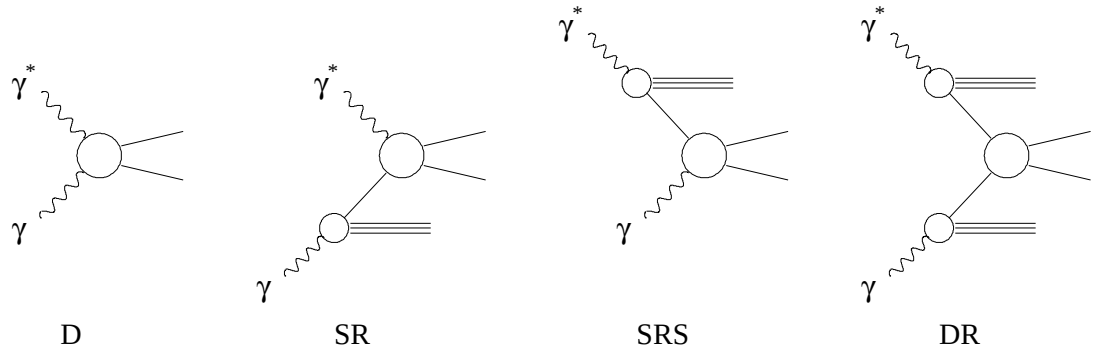

Figure 1: *The different components contributing to jet production in $\gamma^*\gamma$-scattering.*

photon can have a direct and a resolved component. These are called the direct (D) and single-resolved (SR) contributions. In addition to these, the so-called single-virtual resolved (SRS) and double-resolved (DR) contributions occur, when the virtual resolved photon components are included. The four contributions are shown in Fig. 1. In the SRS case, the real photon interacts directly and the virtual photon is resolved. For this case the NLO matrix elements can be taken from photoproduction [12, 13, 14]. Finally, in the DR case both photons are resolved, for which the matrix elements are described in [13]. Since NLO calculations for the case of $\gamma\gamma$-scattering with both photons being on-shell, i.e., $Q^2 \simeq P^2 \simeq 0$, are available in the literature [13, 14, 15], we compare our results in the limiting case $Q^2 \to 0$ with these calculations.

It has been shown in [7, 8, 9] that the parton content of virtual photons is not solely described by purely perturbative contributions in the region $\Lambda^2_{QCD} \ll Q^2 \ll \mu^2$, where μ^2 is the probing scale, in contrast to the expectations from [16]. However, as has been pointed out in [8, 17], it is not clear for which values of Q^2 (and μ^2) the non-perturbative part is relevant and down to which value of Q^2 one should trust perturbation theory. In section 3 we will therefore numerically study the perturbative stability of the $\gamma^*\gamma \to$ jets cross sections in the region $\Lambda^2_{QCD} \ll Q^2 \lesssim E_T^2$, where E_T is the typical hard scale in jet production. We study the K factors for different scales and virtualities and compare the scale dependences of the unsubtracted jet cross sections D and SR with those obtained after the subtraction of the logarithms and inclusion of resolved components SRS and DR. From this comparison we can deduce the regions of photon virtuality where fixed order perturbation theory gives reliable predictions for jet cross sections and where, on the other hand, the parton content of a virtual photon is relevant.

Finally, in section 4, we make predictions for low Q^2 jet production including a virtual resolved photon component as functions of Q^2 and E_T and discuss whether the resolved component can be observed at LEP energies. Further numerical results can be found in [18]. The paper ends with a summary of the results and conclusions.

2 Low Q^2 jet cross sections

Taking over the conventions given in [11], the process we are interested in can be written as

$$e^+(k_a) + e^-(k_b) \longrightarrow e^+(k'_a) + e^-(k'_b) + \text{jets}(E_T) + \text{X} \quad , \tag{1}$$

with the subprocess $\gamma^*(q_a) + \gamma(q_b) \to \text{jets} + \text{X}$, where $q_a = k_a - k'_a$ and $q_b = k_b - k'_b$. The virtualities are given by $Q^2 = -q_a^2$ and $P^2 = -q_b^2 = 0$. The cross section for the process (1) at large Q^2 is given by the convolution

$$\frac{d\sigma_{e^+e^-}}{dQ^2 dy_a dy_b} = \sum_b \int dx_b F_{\gamma/e^-}(y_b) f_{b/\gamma}(x_b) \frac{\alpha}{2\pi Q^2} \left[\frac{1+(1-y_a)^2}{y_a} d\sigma^U_{\gamma^* b} + \frac{2(1-y_a)}{y_a} d\sigma^L_{\gamma^* b} \right] , \tag{2}$$

where $y_a = (q_a k_b)/(k_a k_b)$. The variable $y_b \in [0,1]$ describes the momentum fraction of the real photon in the electron. The momentum fraction of a parton in the real photon is $x_a \in [0,1]$ and the PDF of the real photon is $f_{b/\gamma}(x_b)$. The indices U and L denote the unpolarized and longitudinally polarized virtual photon contributions. Finally, the function $F_{\gamma/e^-}(y_b)$ is the Weizsäcker-Williams approximation for the real photon [19],

$$F_{\gamma/e^-}(y_b) = \frac{\alpha}{2\pi} \frac{1+(1-y_b)^2}{y_b} \ln\left(\frac{E_e^2 \theta_{max}^2}{m_e^2} \right) , \tag{3}$$

where m_e is the electron mass and θ_{max} is the maximum scattering angle of the untagged electron. An improved version of the equivalent-photon approximation in e^+e^- collisions has been derived in [20], leading however only to small corrections. We use the simpler formula (3), since our studies are exploratory and we do not compare with data.

The definition of the partonic cross sections $d\sigma^{U,L}_{\gamma^* b}$ are given in [11]. For the SR case, the NLO calculations can be taken from [21], whereas the NLO calculations for the D case have been presented in [11]; both calculations employ the phase-space-slicing method to extract the singular phase-space regions of the real corrections. The singular integrals of both the real and the virtual corrections are handled in dimensional regularization. Most of the $1/\epsilon^n$ poles for the real and virtual corrections cancel and the remaining initial state corrections are subtracted into the real photon PDF. We are in the following interested in the initial state splitting for the virtual photon, $\gamma^* \to q\bar{q}$, which has been evaluated in [2] for the SR contributions. Here, we repeat this calculation for the D process[1]

$$\gamma^*(q_a) + \gamma(q_b) \to q(p_1) + \bar{q}(p_2) + g(p_3) \ . \tag{4}$$

The first step is to extract from the $2 \to 3$ matrix elements of the reaction (4) a term with the characteristic denominator from the $\gamma^* \to q\bar{q}$ splitting which gives the singular contribution in the limit $Q^2 \to 0$. We call this term H_K. In the same singular

[1]Note, that in [2] the photon virtuality corresponding to our Q^2 was called P^2.

limit the three-body phase space of the $q\bar{q}g$ final state, $d\mathrm{PS}^{(3)}$, factorizes according to $d\mathrm{PS}^{(3)} = d\mathrm{PS}^{(2)} d\mathrm{PS}^{(r)}$, with $d\mathrm{PS}^{(2)}$ being the usual two-body phase-space and $d\mathrm{PS}^{(r)}$ being the phase-space of the the singular region [2, 13, 21]. We define the variable $z_a \equiv (p_2 p_3)/(q_a q_b) \in [\eta_a, 1]$ that gives the fraction of the momentum q_a that participates in the subprocess after a particle has been radiated in the initial state. The variable $\eta_a \in [0, 1]$ is connected to z_a through $\eta_a = x_a z_a$. The term H_K is integrated over the singular phase space up to a cut-off y_s with the result

$$\int d\mathrm{PS}^{(r)} H_K = \frac{\alpha_s}{2\pi} (4\pi\alpha Q_i^2)^2 \int_{\eta_a}^{1} \frac{dz_a}{z_a} \, 2N_C C_F M(Q^2) \; T_\gamma(s,t,u) \quad , \tag{5}$$

where

$$M(Q^2) = \frac{1}{2N_C} P_{q\leftarrow\gamma}(z_a) \ln\left(1 + \frac{y_s s}{z_a Q^2}\right) \tag{6}$$

is the singular term and

$$T_\gamma(s,t,u) = -\frac{s}{u} - \frac{u}{s} \tag{7}$$

is the LO photon-parton scattering matrix element where s, t and u are the usual Mandelstam variables. The photon splitting function is given by $P_{q\leftarrow\gamma}(z_a) = N_C \, (z_a^2 + (1-z_a)^2)$. The term (6) is large for $Q^2 \ll s$ and singular for $Q^2 = 0$, as expected. It is the same universal term as obtained in [2] for the eP-case. We therefore introduce, in accordance with [2], the subtraction term

$$\Gamma_{q\leftarrow\gamma}(z_a, M_\gamma^2) = \ln\left(\frac{M_\gamma^2}{Q^2(1-z_a)}\right) P_{q\leftarrow\gamma}(z_a) - N_C \tag{8}$$

which is to be absorbed into the PDF of the virtual photon. After this subtraction the remaining finite term in $M(Q^2)$ yields

$$M(Q^2)_{\overline{MS}} = -\frac{1}{2N_C} P_{q\leftarrow\gamma}(z_a) \ln\left(\frac{M_\gamma^2 z_a}{(z_a Q^2 + y_s s)(1-z_a)}\right) + \frac{1}{2} \; . \tag{9}$$

In addition to the singular term $\ln(M_\gamma^2/Q^2)$ two finite terms have been subtracted in order to achieve the $\overline{\mathrm{MS}}$ factorization for $Q^2 \neq 0$ [2]. It is defined by the requirement that the remaining finite term $M(Q^2)_{\overline{MS}}$ is equal to the finite term obtained after factorization of the real photon initial state singularities, which can be found in [12, 13, 14]. Of course, this has consequences concerning the selection of the PDF of the virtual photon, the details of which can be found in [2]. This completes the calculation of the contribution from the virtual photon initial state singularity. Note that the above described subtraction only concerns the transversely polarized virtual photons in reaction (4), since the contributions for longitudinal photons vanish in the limit $Q^2 \to 0$. Furthermore, up to now no virtual photon structure function for longitudinal photons has been constructed. The

final formula for jet cross sections including resolved virtual photon contributions in e^+e^- scattering at low Q^2 is a generalization of (1) and reads

$$\frac{d\sigma_{e^+e^-}}{dQ^2 dy_a dy_b} = \sum_{a,b} \int dx_a dx_b F_{\gamma/e^-}(y_b) f_{b/\gamma}(x_b) \frac{\alpha}{2\pi Q^2} \left[\frac{1+(1-y_a)^2}{y_a} f^{vir}_{a/\gamma^*}(x_a, Q^2) d\sigma_{ab} + \frac{2(1-y_a)}{y_a} \delta(1-x_a) d\sigma^L_{\gamma^* b} \right] , \quad (10)$$

where $f^{vir}_{a/\gamma^*}(x_a, Q^2)$ is the virtual photon PDF and $x_a \in [0,1]$ describes the momentum fraction of the parton in the virtual photon. The direct photon interactions are included in this formula through delta functions. For the direct virtual photon one has the relation $f^{vir}_{\gamma^*/\gamma^*} d\sigma_{ab} = \delta(1-x_a) d\sigma^U_{\gamma^* b}$, whereas for the direct real photon the relation is $f_{\gamma/\gamma} d\sigma_{ab} = \delta(1-x_b) d\sigma_{\gamma b}$, where $d\sigma_{ab}$ refers to the partonic cross section.

Formula (10) is implemented in the fixed higher order program `JetViP` [22], with which all numerical results in this paper are produced. The input parameters for all numerical studies are the following. We assume LEP2 conditions, i.e., the energies of the incoming leptons are $E_a = E_b = 91.5$ GeV. We integrate over the full range of $y_a, y_b \in [0,1]$ and use the value $\theta_{max} = 0.025$ in (3). For the real photon we always employ the PDF's of Glück, Reya and Vogt (GRV) [23], whereas for the virtual photon we will use the new GRS [8] parametrization and the SaS1D PDF [9] transformed to the $\overline{\rm MS}$-scheme [2]. The GRS PDF's are constructed for $N_F = 3$ flavours, the production of the heavier c and b quarks is supposed to be added as predicted by fixed order perturbation theory. We calculate our cross sections with $N_F = 5$ flavours and use the two-loop formula for the strong coupling constant without threshold effects with $\Lambda^{(5)}_{QCD} = 153$ MeV, even for the LO results. The cross sections are plotted in the $\gamma^*\gamma$ cms, where also jets are defined. We use the Snowmass accord [24], where two partons i and j are recombined, if for both partons the condition $R_{i,j} < R$ is fulfilled, where $R_{i,J} = \sqrt{(\eta_i - \eta_J)^2 + (\phi_i - \phi_J)^2}$ and η_J, ϕ_J are the rapidity and the azimuthal angle of the combined jet respectively, defined as

$$E_{T_J} = E_{T_1} + E_{T_2} \quad (11)$$

$$E_{T_J}\eta_J = E_{T_1}\eta_1 + E_{T_2}\eta_2 \quad , \quad (12)$$

$$E_{T_J}\phi_J = E_{T_1}\phi_1 + E_{T_2}\phi_2 \quad . \quad (13)$$

We choose $R = 1$.

As a numerical check of our calculations and of the consistency of the $\overline{\rm MS}$-scheme for virtual photons, we compare in Fig. 2 a,b the cross section (10) in the limit $Q^2 \to 0$ with existing calculations for photon-photon scattering [14]. On the virtual photon side, the Q^2 is integrated out by using the Weizsäcker-Williams approximation [19] with $Q^2_{max} = 1$ GeV^2. In Fig. 2 a the comparison is made for $d\sigma/dE_T$ as a function of E_T, where the rapidity has been integrated out in the range $\eta \in [-2,2]$. The dots are the results from Kleinwort and Kramer [14], whereas the curves are the predictions from `JetViP`, for all

four components, D, SR, SRS and DR, as discussed above, now using the SaS PDF's. One sees a perfect agreement. The SR and SRS distributions are very close to each other, but do not coincide exactly, since different PDF's are employed for the real and the virtual photon. However, the SRS and SR cross sections agree exactly on the partonic level. The excellent agreement seen in the E_T distributions holds also for the rapidity distribution $d\sigma/d\eta$ of Fig. 2 b for all four components. The transverse energy in these curves has been integrated out with $E_T > 3$ GeV. The SR and SRS components have their respective maxima at opposite sides of the rapidity range. The SR distribution is peaked at positive η's, since the direction of the virtual photon was taken to be the positive z-axis. In photoproduction, the DR component gives considerable contributions in the low E_T region, as can be seen from the E_T spectra. The D cross section only starts to dominate for E_T larger than 10 GeV. The SR and SRS components are of minor importance.

3 Direct vs. resolved virtual photon approaches

We now compare the two approaches for calculating jet cross sections at small Q^2, namely considering the direct coupling of the virtual photon only and, on the other hand, including the resolved virtual photon components. We cover the region $\Lambda^2_{QCD} \ll Q^2 \lesssim E_T^2$ where one could expect contributions from resolved virtual photons to be of importance. For the discussion in this section we will only use one of the virtual photon PDF's, namely those of SaS, which are built for $N_F = 5$ flavours. The input parameters for the following plots are as described in the previous section.

In Fig. 3 we have plotted the ratio of the single inclusive jet cross sections

$$K = \left(\frac{d\sigma^{NLO}}{dE_T}\right) \Big/ \left(\frac{d\sigma^{LO}}{dE_T}\right) \ , \tag{14}$$

where $d\sigma^{NLO}$ contains all Born terms. The cross sections are obtained by integrating over the rapidity-range $|\eta| < 2$ and for four different values of transverse energy, $E_T = 3, 7, 10$ and 25 GeV, in the region $Q^2 \in [0.1, 200]$ GeV^2, where the lower limit is roughly $Q^2_{min} \simeq 10 \times \Lambda^2_{QCD}$. The renormalization and factorization scales μ_R and μ_F are set equal to E_T. We observe that K is close to unity for all four curves for $Q^2 \gtrsim 30$ GeV^2 which indicates the perturbative stability of the cross sections in the deep-inelastic region. The ratio exceeds 1 below $Q^2 = E_T^2$ and rises monotonically towards smaller Q^2 for the three smaller E_T's. For $E_T = 25$ GeV the NLO terms give only very small corrections below 5% in the whole Q^2 region down to Q^2_{min}. For $E_T = 3$ GeV the rise towards smaller Q^2 is strongest and leads to a NLO correction of nearly 100 % near $Q^2 \simeq Q^2_{min}$, but is already around 50 % for $Q^2 \simeq E_T^2/5$. For the larger E_T values the NLO corrections do not rise that dramatically, however below $Q^2 = 10$ GeV^2 the corrections exceed 20 % for $E_T = 7$ and 10 GeV.

We take out the case $E_T = 3$ GeV to make a more detailed study of the perturbative stability by looking at the scale dependence of the cross sections. In Fig. 4 a–d we show

the single jet inclusive cross section integrated over $|\eta| < 2$ and $E_T > 3$ GeV as a function of $\mu/E_T \in [\frac{1}{3}, 3]$, where $\mu = \mu_R = \mu_F$, i.e., renormalization and factorization scales are varied at the same time. The curves are shown in the four bins of virtuality $Q^2 \in [0.25, 0.5], [1, 2], [2, 5]$ and $[5, 10]$ GeV^2. Since we are interested only in comparing direct and resolved virtual photon contributions, we have introduced the following combinations of the four components D, SR, SRS and DR: the *virtual direct* (VDIR) is the sum of D and SR components, whereas the *virtual resolved* (VRES) is the sum of SRS and DR components. The component labeled VDIR$_S$ is the virtual direct component after subtraction of the term (8) in the D and the corresponding term in the SR component, to be found in [2].

The scale variation of the NLO VDIR contribution between the smallest and largest μ value in Fig. 4 a amounts 30% and goes down to around 15% in the largest Q^2 bin. We have checked that the renormalization scale dependence alone gives a variation of 60% for the smallest and 25% for the largest Q^2 bin, i.e., the scale variation behaviour becomes stable and well behaved for Q^2 approaching E_T^2. Most of the variation with the renormalization scale stems from the SR component, whereas the D component is much more stable and varies at most 10%. This is understandable, since the D component is only $\mathcal{O}(\alpha_s)$ in the strong coupling, whereas the SR component is $\mathcal{O}(\alpha_s^2)$. The rather strong variation of the VDIR component at small Q^2 values together with the large K factor observed above, indicates the need for a resummed approach at small Q^2. We have therefore also plotted the NLO VRES component in Fig. 4 a–d. To avoid double counting, the VRES component can only be added after the perturbative $\gamma^* \to q\bar{q}$ splitting has been subtracted from VDIR (giving VDIR$_S$) since these terms are contained in the pointlike part of the virtual photon PDF. One sees two effects of including the VRES component. First, the scale variation is considerably reduced in the first two Q^2 bins, namely by a factor of 2 in the first bin and even a factor of 4 in the second bin. For the third bin the scale variation of the SUM = VDIR$_S$ + VRES is more or less the same as for the VDIR component alone, i.e., around 20%. For $Q^2 \in [5, 10]$ GeV^2 the SUM prediction becomes unstable for $\mu \lesssim 0.7 E_T$, since in this region $Q^2 > \mu^2$ and the contribution from the virtual photon PDF is very small. But even for $\mu > E_T$ the scale variation of SUM is much larger than for the VDIR alone. The second observation is that including the VRES component in NLO gives a relatively large correction to the pure VDIR component of 20–30%, up to 40% in bin c.

To disentangle the effects of resummation and non-perturbative parts in the virtual photon PDF from those of higher order contributions in the matrix elements we plot in Fig. 5 a–d the same curves as in Fig. 4 a–d with the VRES component in LO only. The sum of NLO VDIR$_S$ and LO VRES gives rather small corrections to the pure VDIR of about 15% in the smallest Q^2-bin and only 5% in bin b. In the bins c and d the two approaches, NLO VDIR and NLO VDIR$_S$+LO VRES, give nearly the same results. The conclusion from this is that the virtual photon PDF is to a very large extent given by the splitting term for $Q^2 > 2$ GeV^2 at $E_T \simeq 3$ GeV, i.e., for $Q^2 \gtrsim \frac{1}{5}\mu^2$. At smaller virtualities one sees effects from resummation and some non-perturbative input. Only small improvements

can be seen from including the VRES component in the bins a and b with respect to the scale variation, in contrast to the findings of Fig. 4. This is however not surprising, since the VRES matrix elements are only LO. Including the VRES parts in NLO reduces the scale dependence, as we have seen above, for bins a and b, i.e., for $Q^2 \lesssim \frac{1}{5}\mu^2$. We have also looked at scale variations of cross sections with larger minimum transverse energy. We find the overall improvement of including a resolved virtual photon component increasingly smaller, the larger the E_T's are. The upper bound $Q^2 \lesssim \frac{1}{5}\mu^2$ for the improvement of the scale dependence is also found for these larger E_T's. As an important result, we found no improvement for $Q^2 > 10$ GeV^2, no matter how large the E_T was. This is also supported by the Q^2-independent small K factor for $E_T = 25$ GeV in Fig. 3. These findings confirm the expectations from [16] that for large enough photon virtualities one should end up with a fully perturbative prediction irrespective of the probing scale.

The bottom line from these observations is that the resolved virtual photon approach improves the scale dependence und thus the perturbative stability of the jet cross sections for $Q^2 < 10$ GeV^2 as long as $Q^2 \lesssim \frac{1}{5}E_T^2$. It is interesting to see that this result, based on perturbative calculations in NLO QCD and without making use of the GRS PDF's, agrees with the restrictions implemented by the GRS group into their old parametrizations of the virtual photon parton densities [7]. Also for the new PDF's [8], for which no restrictions have been implemented, the authors stress that the resolved photon approach is only meaningful for $Q^2 \ll \mu^2$, typically $Q^2 \lesssim \frac{1}{10}\mu^2$. Our results should have some relevance also for jet production at HERA, since the SR and DR contributions, which occur in eP-scattering, are included in this analysis and give considerable contributions. We have checked that the limitations we give above on the Q^2-range for the improvement of the perturbative stability also hold for the SR and DR contributions alone. However, the perturbative stability in the eP-scattering case should be checked in more detail under HERA conditions.

A point one has to keep in mind in this discussion is that the resolved, especially the DR, matrix elements may give important contributions to jet cross sections, even though the non-perturbative input from the virtual photon PDF is small. As we have seen in Fig. 4, the sum of NLO VDIR$_S$ and NLO VRES gives rather large corrections to the NLO VDIR result, even for Q^2, where the photon PDF is given mainly by the pointlike terms. These NLO VRES corrections convoluted with the leading logarithmic contribution to the photon to quark splitting is a leading logarithmic approximation to the full NNLO result with a pure direct virtual photon contribution, which is so far not available. The effect of higher order terms in the resolved matrix elements can be much pronounced in specific phase-space regions, as has been shown in [25]. There, the NLO DR matrix elements are needed to explain the forward jet production cross section at low x_{Bj} in eP-scattering at HERA in the region $Q^2 \in [5, 100]$ GeV^2.

4 Jet cross sections at LEP2

We now turn to predictions of cross sections under conditions to be met at LEP2. We keep the numerical input as specified at the end of section 2. We start with absolute predictions for single jet inclusive cross sections integrated over rapidity $|\eta| < 2$

$$\frac{d\sigma^{1jet}}{dE_T dQ^2} = \int d\eta \frac{d\sigma^{1jet}}{dE_T dQ^2 d\eta} \tag{15}$$

as functions of the transverse energy. In Fig. 6 a–d the spectra are shown for $Q^2 = \frac{1}{10}, 1, 2$ and 5 GeV^2. We have plotted all four components to see their relative importance. To be able to include the resolved contributions we have subtracted the logarithmic terms in the direct components, leading to the D_S (dashed) and SR_S (dash-dotted) curves. One sees the strong fall-off in E_T and the decrease of the absolute values with increasing Q^2. For $Q^2 = 0.1$ GeV^2 the DR component is rather important for the whole shown E_T region and especially dominates at $E_T = 3$ GeV. This is in accordance with the photoproduction results presented in Fig. 2 a. Movin towards larger virtualities, the influence of the DR cross section becomes smaller, and at $Q^2 = 5$ GeV^2 the D component is the dominant contribution. Only for the smallest E_T values is the DR cross section in the same magnitude as the D one. The SR and SRS contributions are always small. In addition, for the SRS cross section a further suppression can be seen for increasing Q^2 due to the suppression of the virtual photon PDF. The virtual resolved components have a stronger fall-off with E_T than the virtual direct contributions and the relative importance of the VRES cross sections diminish with increasing Q^2.

To see in more detail how large the fraction of resolved contributions in the jet cross sections are, we have calculated the ratio of the VRES over the VDIR one-jet inclusive cross sections in LO integrated over $|\eta| < 2$ for three different values $E_T = 3, 5$ and 7 GeV for different virtual photon PDF's as functions of Q^2 in the region $Q^2 \in [0.1, 5]$ GeV^2. Note, that in the LO case no subtraction of the logarithmic terms has to be performed. As a scale we have chosen $\mu_R = \mu_F = E_T$. The results are shown in Fig. 7 a–d. For all three PDF's in Fig. 7 a–c one observes the expected fall off with rising Q^2. The fall off is stronger for the smaller scales. For the larger scales the VRES component diminishes with respect to the VDIR component, but reaches out farther into the larger Q^2 region. For the SaS parametrizations the ratio is around 0.8 below $Q^2 = 0.5$ GeV^2 for $E_T = 3$ GeV and falls off to 0.5 for $E_T = 7$ GeV. At $Q^2 = 5$ GeV the VRES cross section gives about 15–25% of the VDIR one. These results hold also for the SaS2D case, shown in Fig. 7 b, although the SaS1D and SaS2D parametrizations have rather different Q^2-behaviour due to the different evolution starting scales of $Q_0 = 0.6$ GeV and $Q_0 = 2$ GeV, respectively. The SaS2D decreases stronger and is flatter for larger Q^2 than the SaS1D PDF. This can also be seen in Fig. 7 d for the scale $E_T = 5$ GeV, where the two SaS parametrizations can be directly compared as the dashed and the dotted lines. In the same figure also the GRS parametrization [8] (full line) is shown, which produces a still different fall-off behaviour. For the smaller Q^2 the decrease is similar to the SaS2D case but continues

stronger for the larger Q^2. This behaviour is seen for the GRS PDF in Fig. 7 c for all three scales. For comparison we have plotted in Fig 7 d also the old version of the GRS PDF [7] (dash-dotted line), which is rather similar to the new parametrization. It is clear from these curves, especially Fig. 7 d, that the Q^2 dependence is rather different for the GRS and SaS parametrizations which reflects the ambiguities due to the limited data on the virtual photon structure function.

We could repeat the calculation of these ratios for the NLO case, but the VDIR and VRES components alone depend rather strongly on μ_F. Only their sum is independent from μ_F. It is preferable to adopt the strategy used experimentally to distinguish direct and resolved cross sections for dijet events. The OPAL collaboration have presented distributions in $x_\gamma^\pm$ for $\gamma\gamma$-scattering [26], where

$$x_\gamma^\pm = \frac{\sum_{jets}(E \pm p_z)}{\sum_{hadrons}(E \pm p_z)}. \tag{16}$$

The sum in the numerator runs over the two largest E_T jets in the event. The direct dominated cross sections then corresponds to those contributions, where $x_\gamma^\pm > 0.8$ and the resolved dominated correspond to $x_\gamma^\pm < 0.8$. The comparisons with NLO calculations show good agreement [13]. We however do not show curves like this here since it is not clear whether the statistics in the $\gamma^*\gamma$-case will be high enough to extract such distributions.

Instead, we compare absolute single-jet cross sections like (15) for the pure VDIR and the VDIR$_S$+RES approaches with different virtual photon PDF's GRS and SaS, which are shown in Fig. 8 a–d. For $Q^2 = 0.1$ GeV^2 the VRES approach yields about a factor of 2 larger cross sections. This is expected, since this small virtuality lies in the photoproduction domain. The predictions from the SaS and the GRS PDF's give similar results. However, for $Q^2 = 1$ GeV^2 these two parametrizations already give rather different predictions. The GRS curve is for the smaller E_T's around 50% larger than the VDIR, whereas the SaS is 70% larger. Furthermore, the SaS curves do not fall off that strong with increasing E_T. In Fig. 8 c, the difference between the two VRES predictions is quite pronounced. At $Q^2 = 5$ GeV^2, the SaS curve gives still a 30–40% larger cross section than the VDIR, whereas the GRS curve yields basically the same result as the VDIR. In general, the difference between the VRES and the VDIR cross sections in the low Q^2 region is large enough that it should be possible to distinguish between these two approaches experimentally. Furthermore, the difference between the VRES curves with the SaS and GRS parametrizations is rather large and it should therefore also be possible to distinguish between these specific PDF's and to constrain the Q^2-dependence of the virtual photon PDF.

5 Summary

We have presented a calculation of jet cross sections in $\gamma^*\gamma$ scattering from e^+e^--collisions at low Q^2 in NLO QCD, employing the phase-space slicing method to extract singularities

in the real corrections. Logarithmic contributions from the virtual photon initial state have been subtracted and absorbed into the resolved virtual photon structure function. Comparison with existing photoproduction calculations in the limit $Q^2 \to 0$ showed very good agreement.

We have studied the perturbative stability of two approaches to low Q^2 jet production, namely the pure direct coupling of virtual photons and, secondly, the inclusion of resolved virtual photons by looking at K factors and scale dependences. We found the resolved virtual photon approach to improve the perturbative stability for $Q^2 < 10$ GeV^2 with $Q^2 \lesssim \frac{1}{5}E_T^2$. However, the NLO corrections to the resolved matrix elements may be important also for larger Q^2.

We further made predictions for inclusive jet production at LEP2 and found that it should be suitable to experimentally distinguish between different parametrizations of the virtual photon structure functions, since the DR contributions are rather important at low Q^2. It should also be possible to restrict the Q^2 dependence of the parametrizations by comparing the data to the predictions for E_T spectra of the jet cross sections.

References

[1] M. Glück, E. Reya, M. Stratmann, Phys. Rev. D54 (1996) 5515;
D. de Florian, C. Garcia Canal, R. Sassot, Z. Phys. C75 (1997) 265;
J. Chyla, J. Cvach, Proceedings of the Workshop 1995/96 on "Future Physics at HERA", eds. G. Ingelman, A. de Roeck and R. Klanner, DESY 1996, Vol. 1, p. 545

[2] M. Klasen, G. Kramer, B. Pötter, Eur. Phys. J. C1 (1998) 261;
B. Pötter, DESY-97-138, hep-ph/9707319

[3] G. Kramer, B. Pötter Eur. Phys. J. C5 (1998); see also [4], p. 29, hep-ph/9810450

[4] Proceedings of the Workshop on "Photon interactions and the photon structure", Lund, Sweden, 10-12 September 1998, eds. G. Jarlskog and T. Sjöstrand

[5] H1 Collaboration (C. Adloff et al.), Phys. Lett. B415 (1997) 418; DESY-98-076, hep-ex/9806029; DESY-98-205, hep-ex/9812024;
ZEUS Collaboration (J. Breitweg et al.), 29th International Conference on High Energy Physics (ICHEP98), Vancouver, Canada, 23-29 July 1998

[6] PLUTO Collaboration (Ch. Berger et al.), Phys. Lett. B142 (1984) 119

[7] M. Glück, E. Reya, M. Stratmann, Phys. Rev. D51 (1995) 3220

[8] M. Glück, E. Reya, I. Schienbein, DO-TH 99/03, February 1999, hep-ph/9903337

[9] G.A. Schuler, T. Sjöstrand, Z. Phys. C68 (1995) 607; Phys. Lett. B376 (1996) 193

[10] OPAL Collaboration, OPAL physics note PN293, May 1997. Contribution to XVIII Intern. Symposium on Lepton-Photon Interactions, Hamburg 1997 and to the Intern. Europhysics Conference om HEP, Jerusalem 1997

[11] B. Pötter, Nucl. Phys. B540 (1999) 382

[12] M. Klasen, G. Kramer, Z. Phys. C72 (1996) 107

[13] M. Klasen, T. Kleinwort, G. Kramer, EPJ direct 1 (1998) 1

[14] T. Kleinwort, G. Kramer, Nucl. Phys. B477 (1996) 3; Phys. Lett. B370 (1996) 141; Z. Phys. C75 (1997) 489; T. Kleinwort, DESY-96-165

[15] P. Aurenche, J.-Ph. Guillet, M. Fontannaz, Y. Shimizu, J. Fujimoto, K. Kato, Progr. Theor. Phys. 92 (1994) 175;
L.E. Gordon, Nucl. Phys. B419 (1994) 25

[16] T. Uematsu, T.F. Walsh, Phys. Lett. B101 (1981) 263, Nucl. Phys. B199 (1982) 93; G. Rossi, Phys. Rev. D29 (1984) 852

[17] M. Stratmann, contribution to [4], p. 183, hep-ph/9811260

[18] B.Pötter, contribution to [4], p. 175, hep-ph/9810466; Proceedings of International Euroconference on Quantum Chromodynamics (QCD 98), Montpellier, France, 2-8 July 1998, hep-ph/9807538

[19] C.F. v. Weizsäcker, Z. Phys. 88 (1934) 612; E.J. Williams, Kgl. Danske Vidensk. Selskab. Mat-Fiz. Medd. 13 (1935) N4

[20] G.A. Schuler, CERN-TH/96-297, October 1996, Phys. Lett. B (in press)

[21] D. Graudenz, Phys. Rev. D49 (1994) 3291

[22] B. Pötter, DESY-98-071, hep-ph/9806437, Comp. Phys. Comm. (in press)

[23] M. Glück, E. Reya, A. Vogt, Phys. Rev. D45 (1992) 3986; Phys. Rev. D46 (1992) 1973

[24] J.E. Huth et al., Proc. of the 1990 DPF Summer Study on High Energy Physics, Snowmass, Colorado, edited by E.L. Berger, World Scientific, Singapore, 1992, p. 134

[25] G. Kramer, B. Pötter, DESY-99-004, MPI–PhT 99-01, hep-ph/9901314

[26] OPAL Collaboration, OPAL physics note 291, May 1997. Contribution to XVIII Intern. Symposium on Lepton-Photon Interactions, Hamburg 1997; Proceedings of the Ringberg Workshop on "New Trends in HERA Physics", Ringberg 1997.

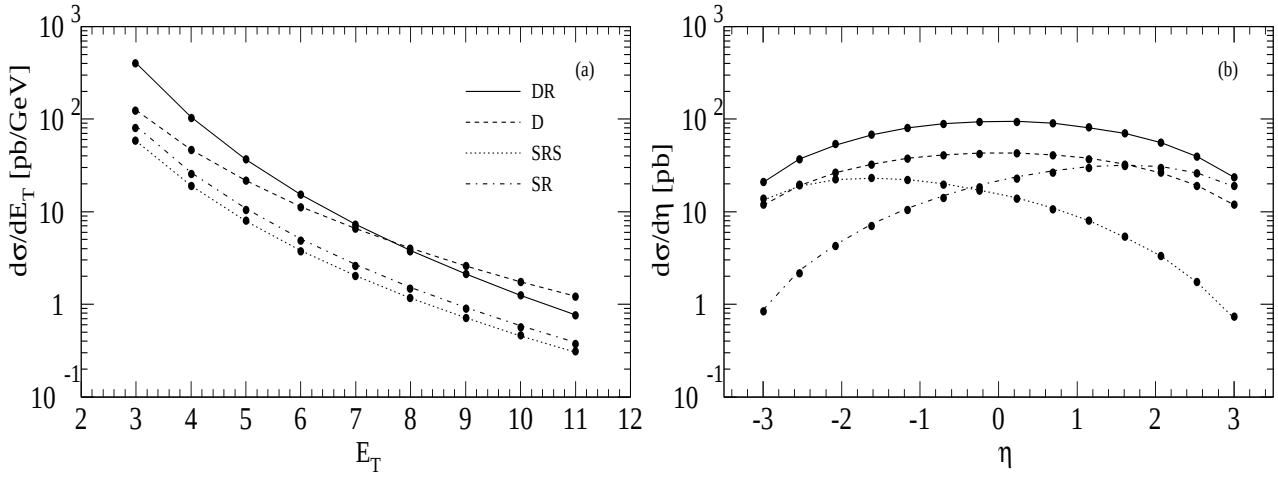

Figure 2: *Comparison of single inclusive jet cross sections in the limit* $Q^2 \to 0$ *(lines) with the calculations of Kleinwort and Kramer (dots). The full lines give the DR, the dashed the D, the dotted the SRS and the dash-dotted the SR contributions. (a)* E_T *distribution with* $|\eta| < 2$*; (b)* η *distribution with* $E_T > 3$ *GeV.*

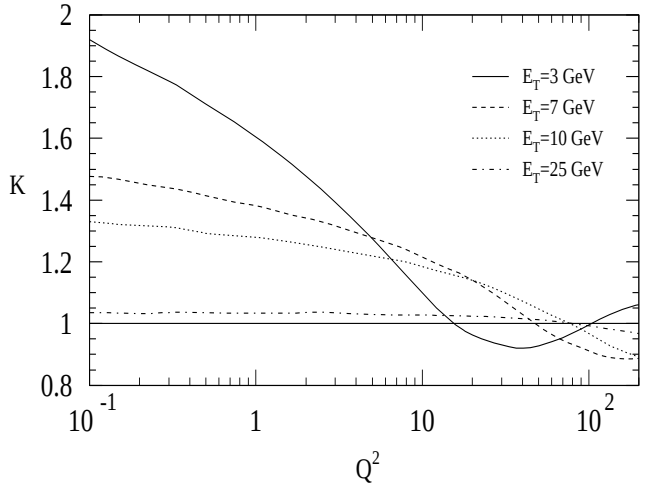

Figure 3: *Ratio of NLO to LO single jet cross sections integrated over* $|\eta| < 2$ *for* $E_T = 3, 7, 10$ *and* 25 *GeV as a function of* Q^2*.*

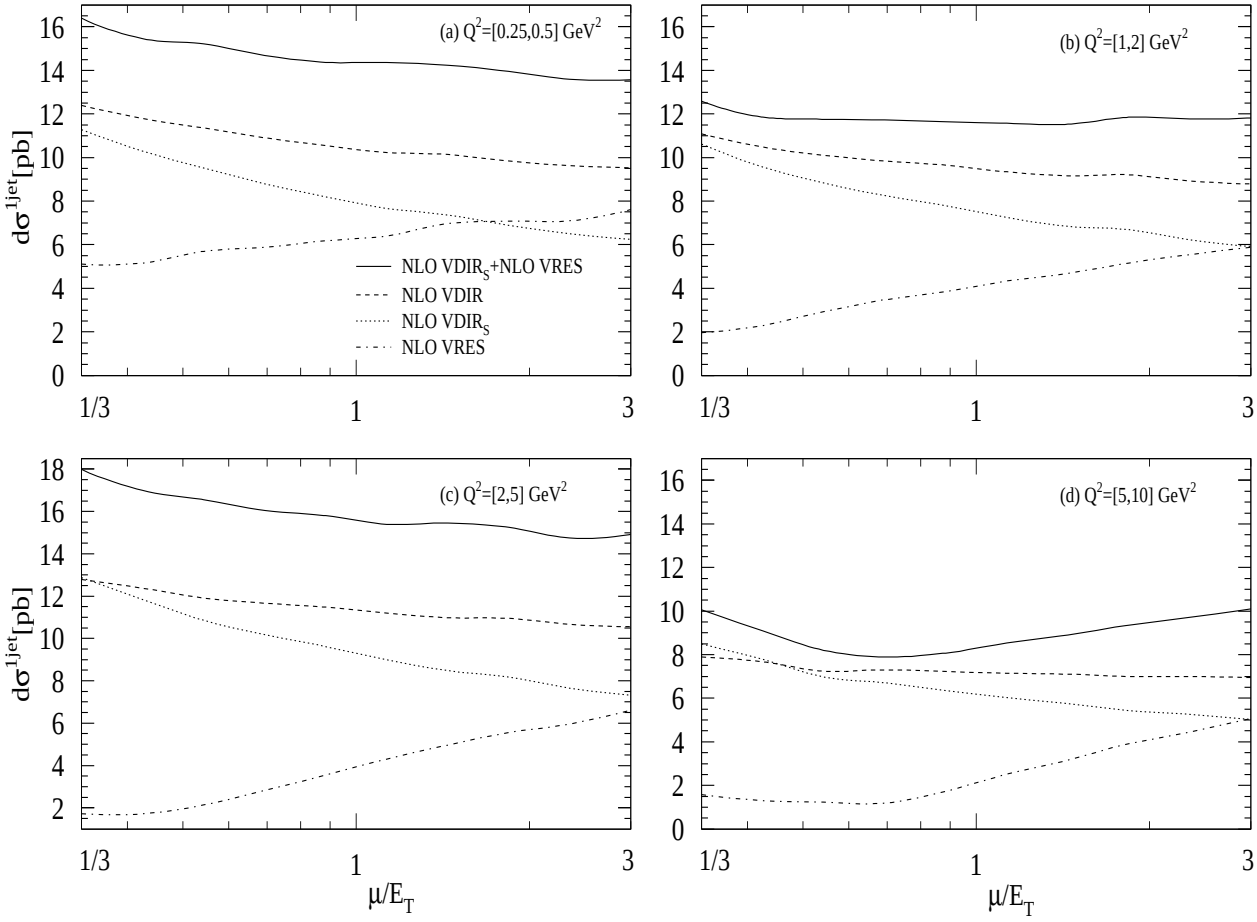

Figure 4: *Scale dependences of single inclusive jet cross sections integrated over* $|\eta| < 2$ *and* $E_T > 3$ *GeV as a function of* μ/E_T *for (a)* $Q^2 \in [\frac{1}{4}, \frac{1}{2}]$ *GeV², (b)* $Q^2 \in [1, 2]$ *GeV², (c)* $Q^2 \in [2, 5]$ *GeV² and (d)* $Q^2 \in [5, 10]$ *GeV². The dashed line is the NLO VDIR which has to be compared with the full line, giving the sum of the subtracted virtual direct (NLO* $VDIR_S$*, dotted line) and the NLO virtual resolved (NLO VRES, dash-dotted line).*

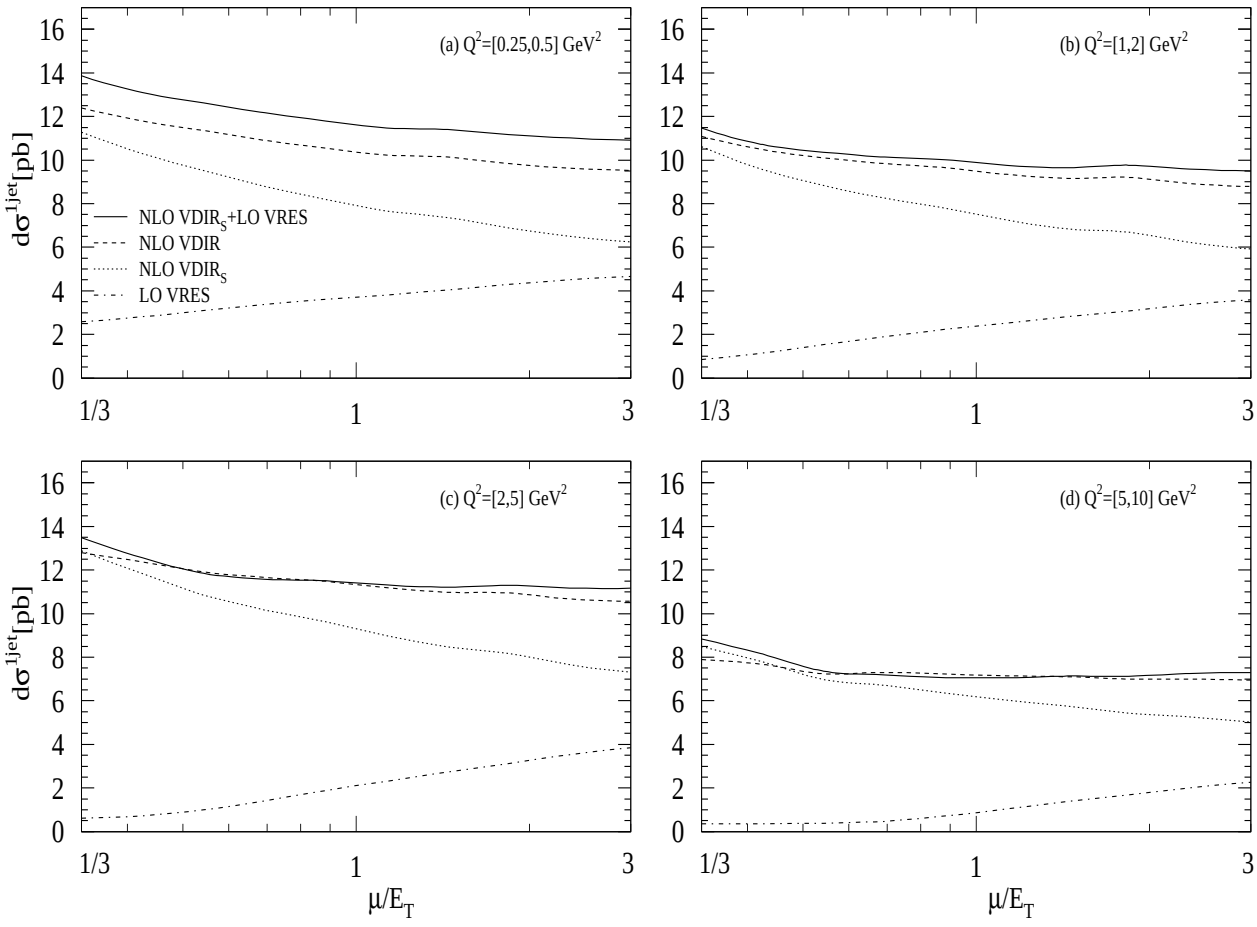

Figure 5: *Scale dependences of single inclusive jet cross sections with the same conditions as in Fig. 4 a–d, only here the virtual resolved contribution is included in LO instead of NLO.*

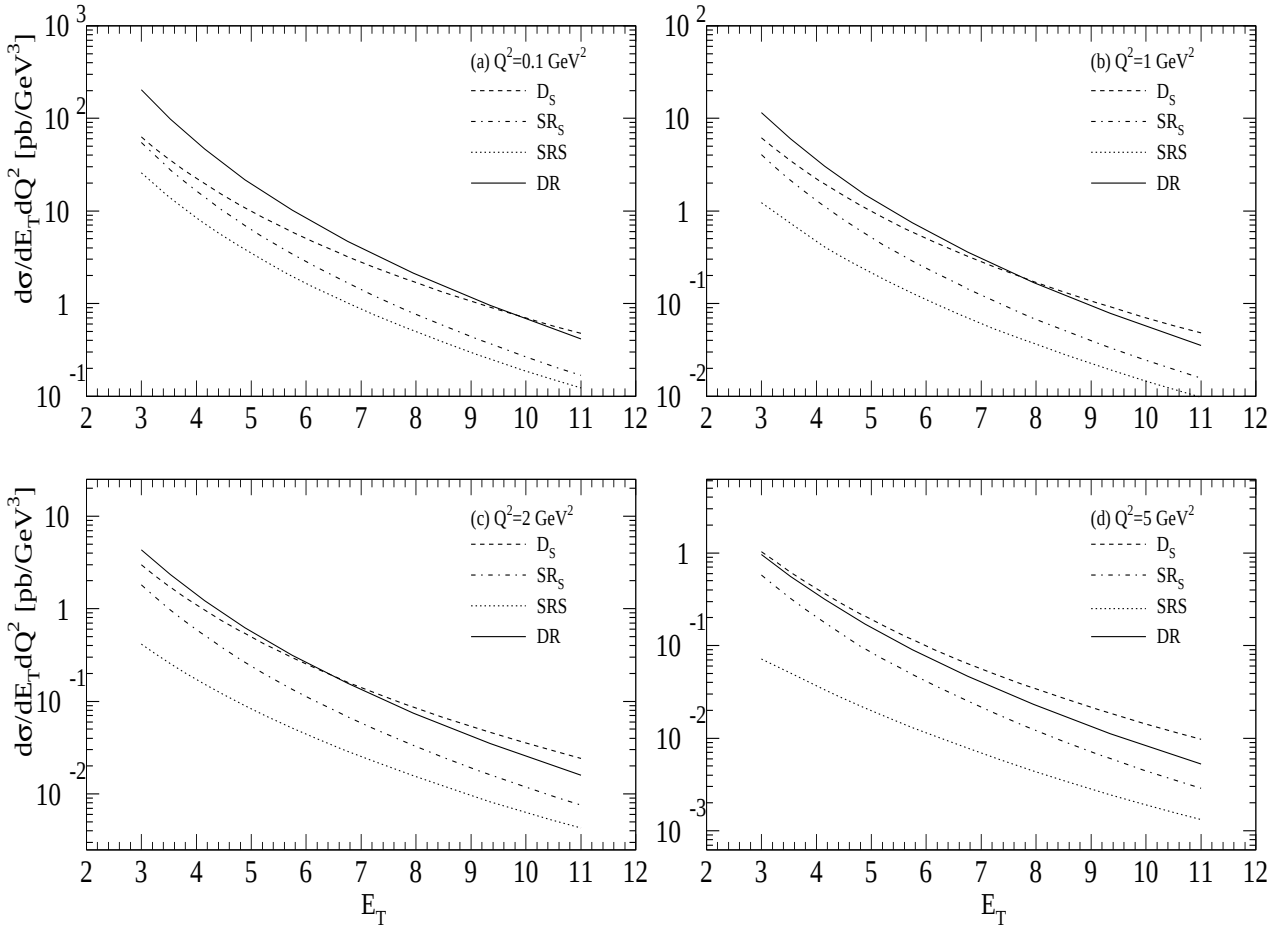

Figure 6: *NLO single jet inclusive cross sections integrated over* $|\eta| < 2$ *as functions of* E_T *for different virtualities, employing the SaS PDF's. (a)* $Q^2 = 0.1\ GeV^2$*; (b)* $Q^2 = 1\ GeV^2$*; (c)* $Q^2 = 2\ GeV^2$*; (d)* $Q^2 = 5\ GeV^2$*.*

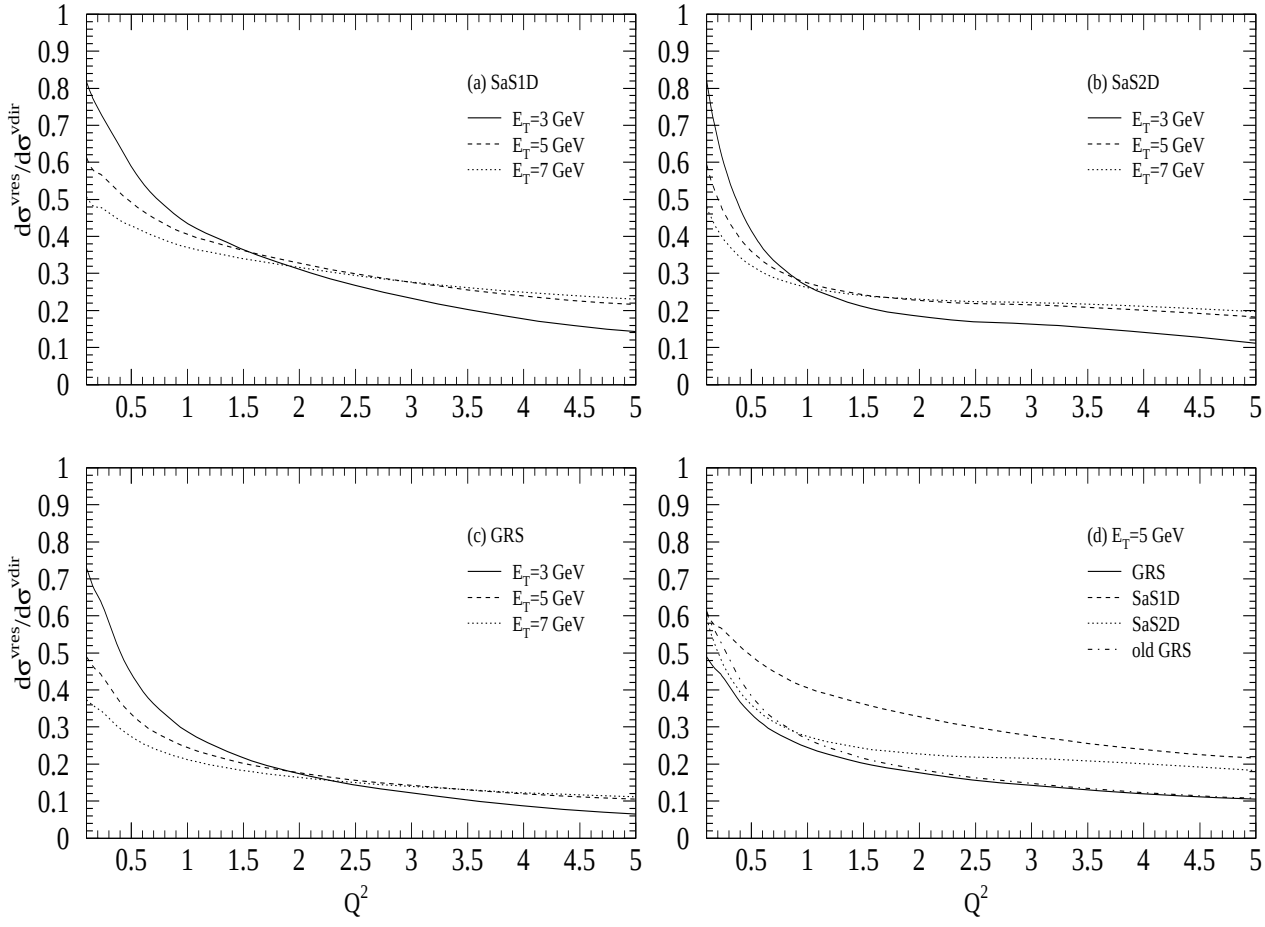

Figure 7: *LO ratio of VRES over VDIR of one-jet inclusive cross sections, integrated over* $|\eta| < 2$ *for three different scales* $E_T = 3, 5$ *and* 7 *GeV for different virtual photon PDF's. (a) SaS1D; (b) SaS2D; (c) GRS; (d) comparing the PDF's from a–c at* $E_T = 5$ *GeV together with the old GRS PDF.*

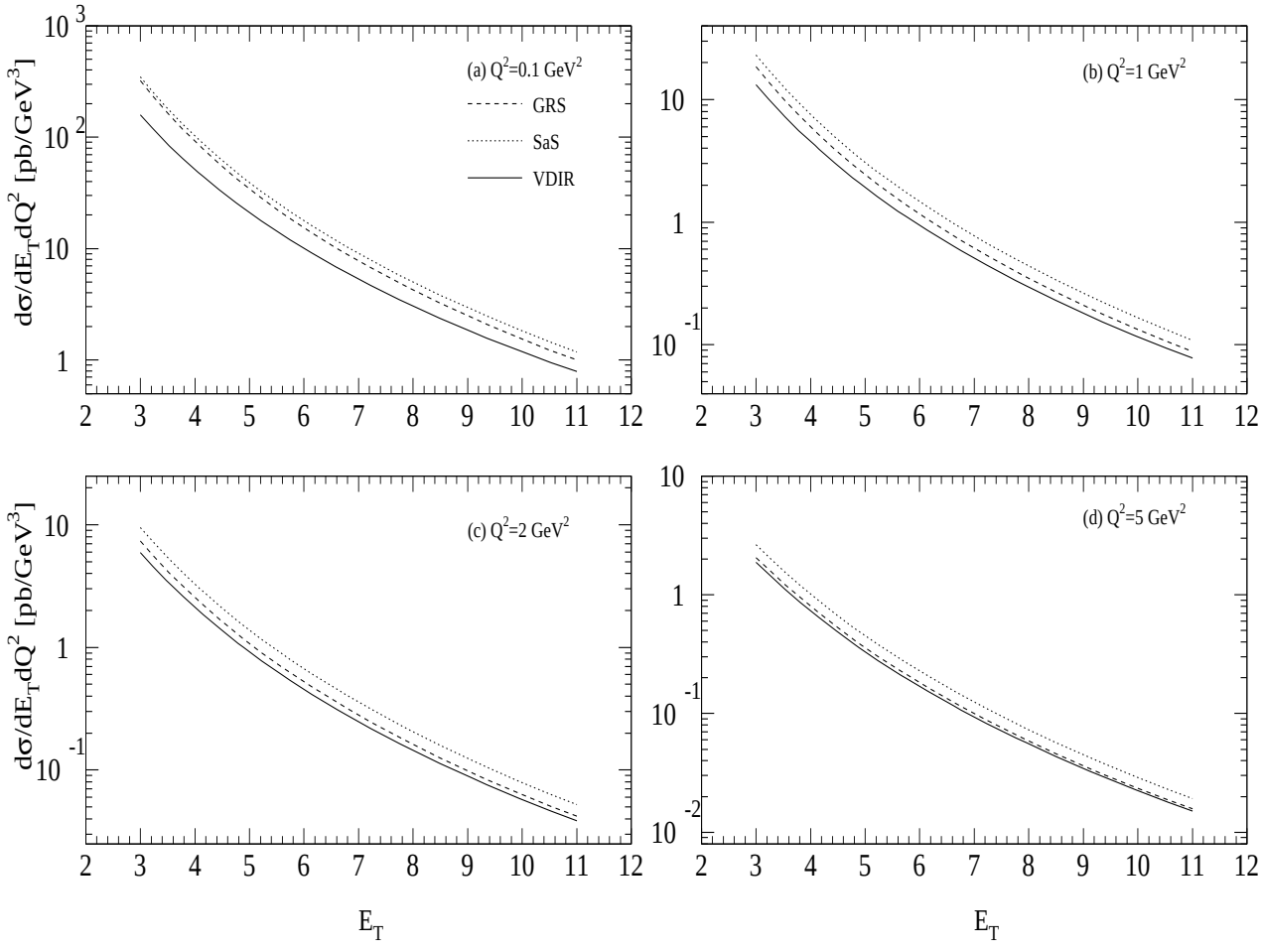

Figure 8: *NLO single jet inclusive cross sections integrated over $|\eta| < 2$ as functions of E_T for Q^2 values as in Fig. 6 a–d; the full line gives the unsubtracted direct (DIS) and has to be compared with the curves denoted GRS and SaS. These are the sum of NLO subtracted direct and NLO resolved cross sections, employing the GRS (dashed) or the SaS (dotted) parton densities.*